NATURAL RESOURCES

TSUNAMI INUNDATION, CURRENT SPEEDS, AND ARRIVAL TIMES SIMULATED FROM AN M_w 9.2 ALASKA-ALEUTIAN SUBDUCTION ZONE EARTHQUAKE SCENARIO FOR COASTAL WASHINGTON

by Alexander Dolcimascolo, Daniel W. Eungard, Alexander N. Steely,
Randall J. LeVeque, Loyce M. Adams, Vasily V. Titov,
Christopher Moore, and Diego Arcas

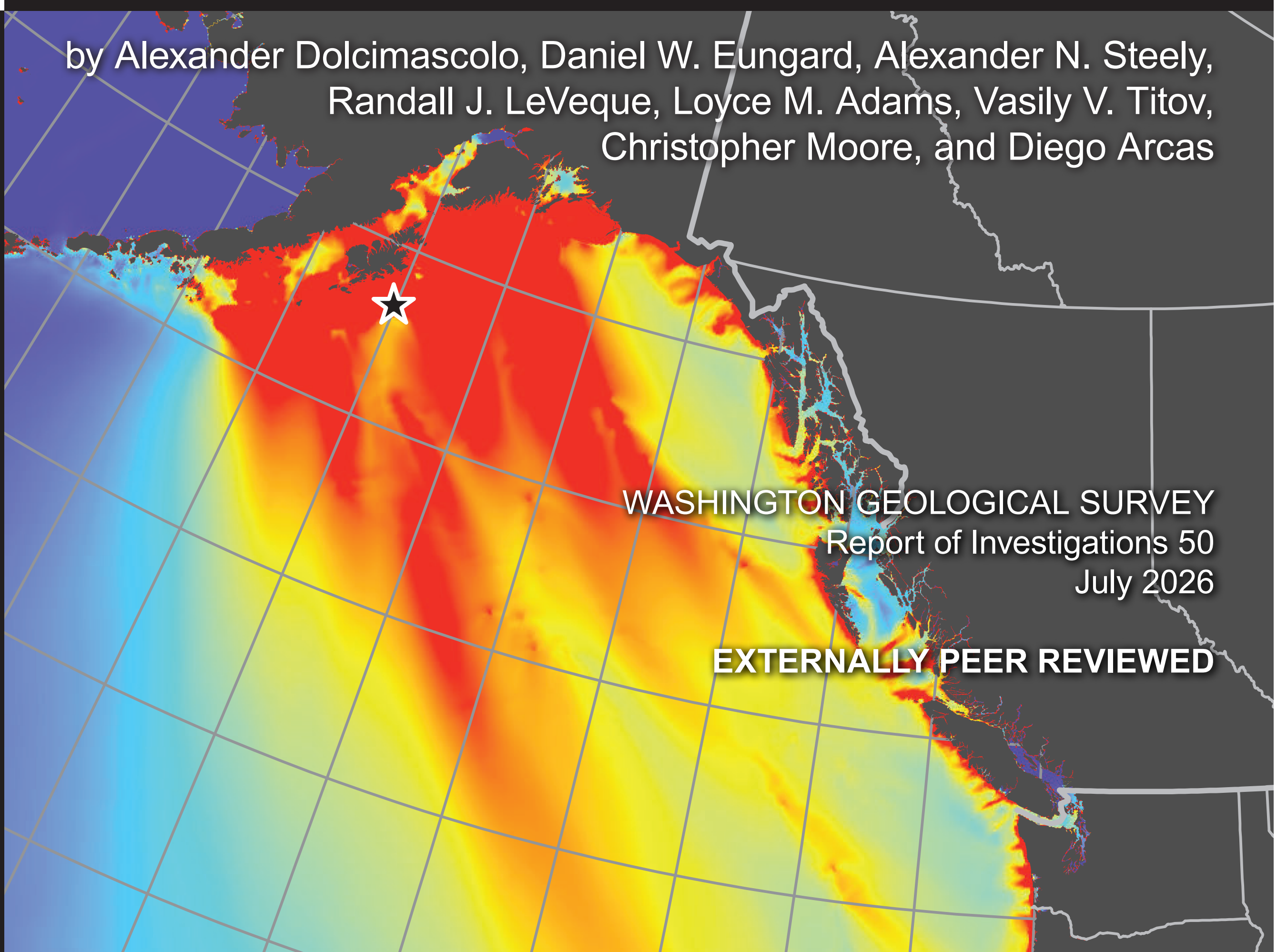

WASHINGTON GEOLOGICAL SURVEY
Report of Investigations 50
July 2026

EXTERNALLY PEER REVIEWED

WASHINGTON STATE DEPARTMENT OF
NATURAL RESOURCES
WASHINGTON GEOLOGICAL SURVEY

TSUNAMI INUNDATION, CURRENT SPEEDS, AND ARRIVAL TIMES SIMULATED FROM AN M_W 9.2 ALASKA-ALEUTIAN SUBDUCTION ZONE EARTHQUAKE SCENARIO FOR COASTAL WASHINGTON

by Alexander Dolcimascolo, Daniel W. Eungard, Alexander N. Steely, Randall J. LeVeque, Loyce M. Adams, Vasily V. Titov, Christopher Moore, and Diego Arcas

WASHINGTON GEOLOGICAL SURVEY
Report of Investigations 50
July 2026

This report was funded by NOAA Awards #NA18NWS4670080, #NA19NWS4670017, and #NA20NWS4670068. This does not constitute an endorsement by NOAA.

This article has undergone a refereed review process with input from three of the authors' subject-matter peers from outside the Washington Geological Survey who did not contribute to the writing of the article.

This publication has also been subject to an iterative review process with Survey editors and has been formatted by Survey staff.

WASHINGTON STATE DEPARTMENT OF
NATURAL RESOURCES
WASHINGTON GEOLOGICAL SURVEY

INDEMNIFICATION

This report was funded by NOAA Awards #NA18NWS4670080, #NA19NWS4670017, and #NA20NWS4670068.
This does not constitute an endorsement by NOAA.

Washington State Department of Natural Resources
Washington Geological Survey

Mailing Address:
1111 Washington St SE
MS 47007
Olympia, WA 98504-7007

Street Address:
Natural Resources Bldg, Rm 148
1111 Washington St SE
Olympia, WA 98501

Phone: 360-902-1450
Fax: 360-902-1785
Email: geology@dnr.wa.gov
Website: www.dnr.wa.gov/geology

WGS Website

Publications and Maps:
www.dnr.wa.gov/programs-and-services/geology/publications-and-data/publications-and-maps

Washington Geology Library Searchable Catalog:
www.dnr.wa.gov/programs-and-services/geology/washington-geology-library

Suggested Citation: Dolcimascolo, Alexander; Eungard, D. W.; Steely, A. N.; LeVeque, R. J.; Adams, L. M.; Titov, V. V.; Moore, Christopher; Arcas, Diego, 2026, Tsunami inundation, current speeds, and arrival times simulated from an M_W 9.2 Alaska-Aleutian subduction zone earthquake scenario for coastal Washington: Washington Geological Survey Report of Investigations 50, 17 p. [https://fortress.wa.gov/dnr/geologydata/tsunami_hazard_maps/ger_ri50_alaska_tsunami_washington.pdf]

Cover: Figure 9 from this report. Modeled tsunami maximum wave amplitudes.

State of Washington
Engineering Geologist
3151
Licensed Geologist
Daniel Eungard

July 2026

Contents

FIGURES

TABLES

DATA SUPPLEMENT

Digital data download package (Zip file, 5.4 GB) containing:

- Rasters of flow depth, current velocity, and momentum flux
- Shapefiles of inundation extent and arrival time points
- Technical reports that accompany each model project
- A readme file

[https://fortress.wa.gov/dnr/geologydata/tsunami_models/WGS_Washington_AK9p2_model_data.zip]

Tsunami Inundation, Current Speeds, and Arrival Times Simulated from an M_W 9.2 Alaska-Aleutian Subduction Zone Earthquake Scenario for Coastal Washington

by Alexander Dolcimascolo[1], Daniel W. Eungard[1], Alexander N. Steely[1], Randall J. LeVeque[2], Loyce M. Adams[2], Vasily V. Titov[3], Christopher Moore[3], and Diego Arcas[3]

[1] Washington Geological Survey
1111 Washington St SE
MS 47007
Olympia, WA 98504-7007

[2] Department of Applied Mathematics
University of Washington
Lewis Hall #201, Box 353925
Seattle, WA 98195-3925

[3] Pacific Marine Environmental Laboratory
NOAA/R/PMEL
7600 Sand Point Way NE
Seattle, WA 98115

ABSTRACT

This report is a compilation of tsunami modeling results based on a hypothetical magnitude 9.2 earthquake along the Alaska-Aleutian subduction zone that would produce a tsunami impacting Washington. We present new and existing inundation and current-speed models for all of coastal Washington. This tsunami modeling was a collaborative effort between the NOAA Center for Tsunami Research at the Pacific Marine Environmental Laboratory, the Tsunami Modeling Group within the Department of Applied Mathematics at the University of Washington, and the Washington Geological Survey. Each group modeled a tsunami generated from an earthquake with a uniform slip of 65.6 ft (20 m) centered on the subduction zone offshore Kodiak Island, Alaska. An event of this size would generate an M_W 9.2 earthquake and has an estimated recurrence interval of ~600 yrs. We chose to center the event in a location that would maximize the wave energy directed at the Washington coastline, as shown by previous modeling efforts. Thus, the inundation depth and inundation extent results presented for a tsunami arriving at high tide (MHW) and without considering future sea level change are likely the maximum expected from an earthquake of this magnitude on the Alaska-Aleutian subduction zone.

The first modeled tsunami wave arrives in the form of a rising (cresting) wave off the coast of Washington just over three and a half hours after the start of the earthquake. This categorizes the tsunami as a distant source event having greater than three hours travel time to Washington. This tsunami wave also propagates into the Strait of Juan de Fuca and adjacent inner waterways, eventually reaching both Olympia in the south Sound and the Washington-Canadian Border in Whatcom County. Tsunami activity may last for up to 24 h or more and the first wave may not be the largest or produce the most inundation. The largest offshore wave amplitudes (height above MHW datum) occur along the outer coast near Westport, exceeding 20 ft (6 m) just offshore. The greatest inundation depths occur along the outer coast, within Grays Harbor and Willapa Bay, where inundation depth at the shoreline is ~10 ft (3 m) and decreases inland. While the outer coast is the most impacted by a distant Alaska tsunami, Washington's inner waterways also face some risk, particularly from fast currents induced by the tsunami. Inner coast locations such as the San Juan Islands, Guemes Channel, Port Gamble, and Hood Canal should expect hazardous current speeds, which pose particular risk to mariners and maritime infrastructure.

Our modeling does not account for changing tides, tidal currents, river flow, seiches, or topographic changes such as grading or natural erosion and deposition that has occurred since the model was run that would locally modify the effects of tsunami waves. In addition, there are many assumptions associated with the modeled seismic scenario. Due to the regional scale of this modeling, the results are not suitable for site-specific tsunami inundation assessment, or for determining effects on the built environment. Despite its limitations, our modeling helps to raise awareness of the hazards from a distant-source tsunami and can be a useful tool for land use planning, emergency preparation, and evacuation planning. Our modeling shows that damaging tsunamis can impact Washington from a distant-source event and highlights the need for prompt and effective notifications and alerts.

INTRODUCTION

The Alaska-Aleutian subduction zone (AASZ) is about 2,500 mi (4,000 km) long, from the Gulf of Alaska to the Kamchatka Peninsula in the Pacific Ocean. The AASZ is a plate boundary where, in the area of Kodiak Island, the Pacific plate subducts beneath the North American continental plate at a relative rate of ~60 mm/yr (DeMets and others, 2010). The AASZ is very seismically active and has the potential to generate large earthquakes and tsunamis. Since the year 1788, as many as 82 tsunamis have been observed and attributed to the AASZ (Wesson and others, 2007). This includes the 1964 M_W 9.2 Great Alaska Earthquake, which generated a tsunami that not only devastated the Alaskan coastline (Plafker and Kachadoorian, 1966) but also caused destruction and fatalities along the coastlines of British Columbia, Washington, Oregon, and California (Lander and others, 1993). This earthquake was the second largest ever recorded since modern seismic instrumentation was introduced in the early 1900s.

Out of all subduction zones located along the Pacific Rim, the AASZ is Washington's greatest distant-sourced (travel time greater than 3 h) tsunami hazard. When considering all earthquake scenarios for this region within the NOAA short-term inundation forecasting for tsunamis (SIFT) propagation database (Gica and others, 2008; http://sift.pmel.noaa.gov/ComMIT/compressed/info_sz.dat), we chose the scenario that produces the maximum wave energy directed at the Washington coastline. Unlike an earthquake on the nearby Cascadia Subduction Zone or a local crustal fault (referred to as a 'local source'), an earthquake on the AASZ (a 'distant source') does not produce any land-level changes in Washington. The distance to the source also means that any shaking during the earthquake may not be felt, and thus it is critical for tsunami warnings to be disseminated by local officials.

In this publication, we present tsunami-modeling results for all of coastal Washington (Fig. 1) based on an earthquake comparable in magnitude to the 1964 Great Alaska Earthquake. To do this, we combined outputs from multiple tsunami hazard assessments into a single statewide dataset. This dataset provides inundation extent, inundation depth, current velocity, momentum flux, and tsunami arrival times for the same hypothetical M_W 9.2 earthquake source with detailed GIS available in a Data Supplement.

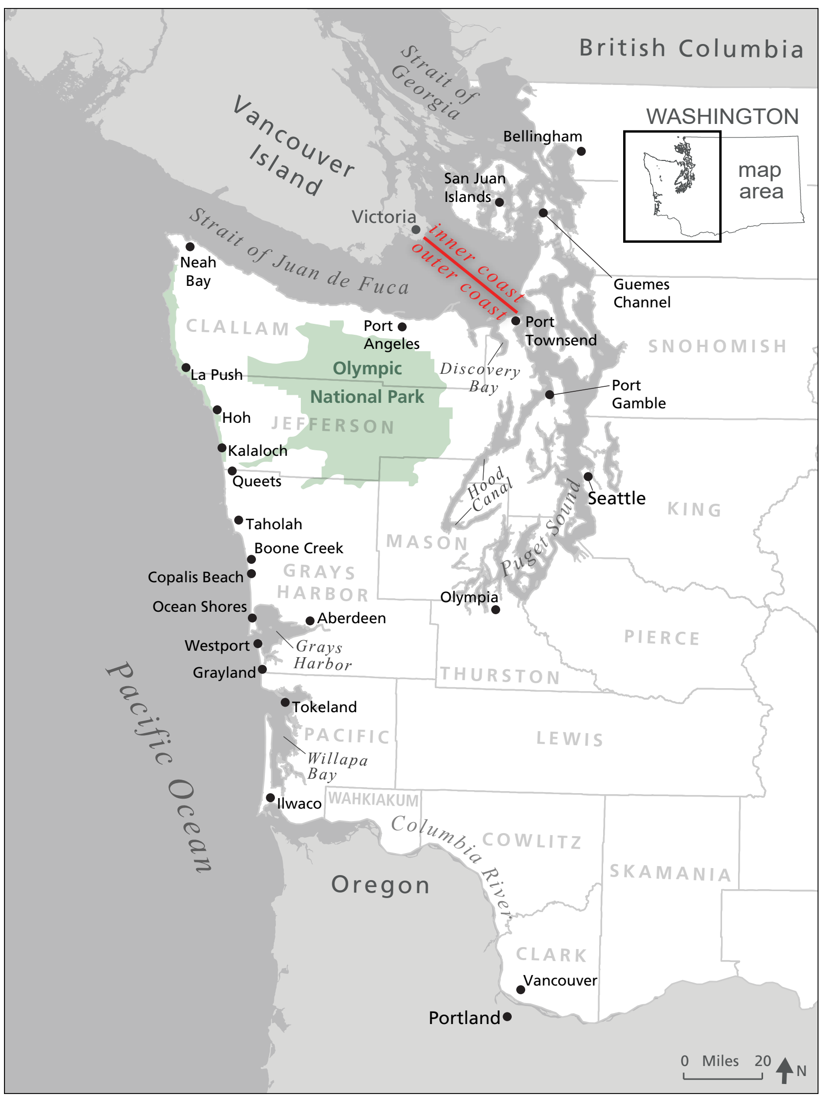

Figure 1. Map of the study area, the Washington coastline from British Columbia to the Columbia River.

Alaska-Aleutian Subduction Zone Seismicity and Directivity

The AASZ is particularly hazardous due to its historical seismicity. This seismicity includes 11 $M_W \geq 8$ earthquakes and 38 M_W 7–8 earthquakes since 1900 (National Geophysical Data Center/World Data Service, 2025). Large magnitude 9+ earthquakes, such as the 1964 earthquake (Fig. 2), are less common and no other similar events have occurred in historical time. Of these historical events, no earthquakes of equivalent size to the 1964 earthquake ocurred along the part of the subduction zone that directs the greatest energy toward Washington.

Impacts from the 1964 Tsunami in Washington

Historically, the only significant tsunami from Alaska to impact Washington was produced by the M_W 9.2 Great Alaska Earthquake, sometimes referred to as the Good Friday earthquake, which struck Prince William Sound and south-central Alaska on Good Friday, March 27, 1964 (National Geophysical Data Center/World Data Service, 2025). This earthquake generated a major tsunami that disrupted infrastructure along the outer coast of Washington. The tsunami, initiated at 3:36 UTC (7:36 pm PST), traveled south from Alaska and reached Neah Bay just after 7:00 UTC (11 pm PST) on a rising tide (Fig. 3). The tsunami wave front propagated southward along the coast and reached the mouth of the Columbia River approximately 3.5 to 4 h after the earthquake (~11–11:30 pm PST). Locally generated debris was deposited along shorelines in Clallam, Grays Harbor, and Pacific Counties. Description of significant impacts of the 1964 tsunami

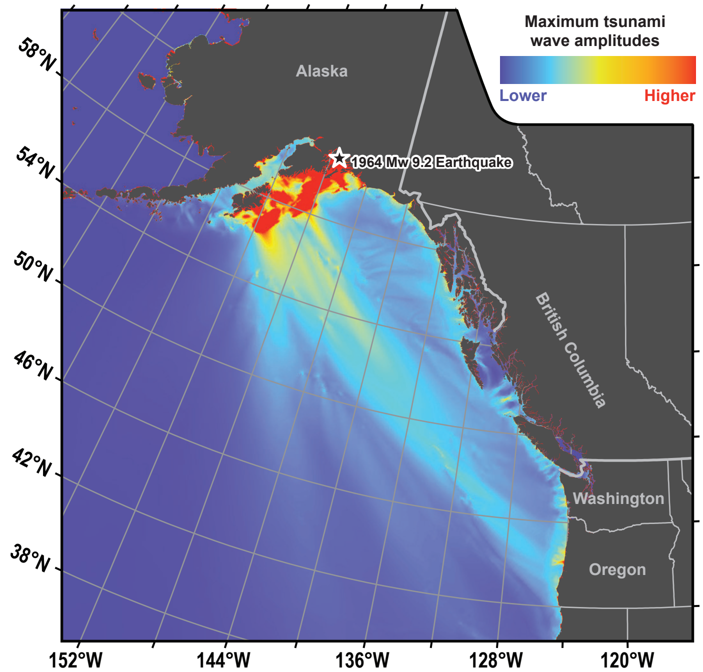

Figure 2. Modeled tsunami maximum wave amplitudes from an Alaska 1964 source model described in Suleimani (2011). Wave amplitudes are commonly used as a proxy for propagation and directivity of wave energy.

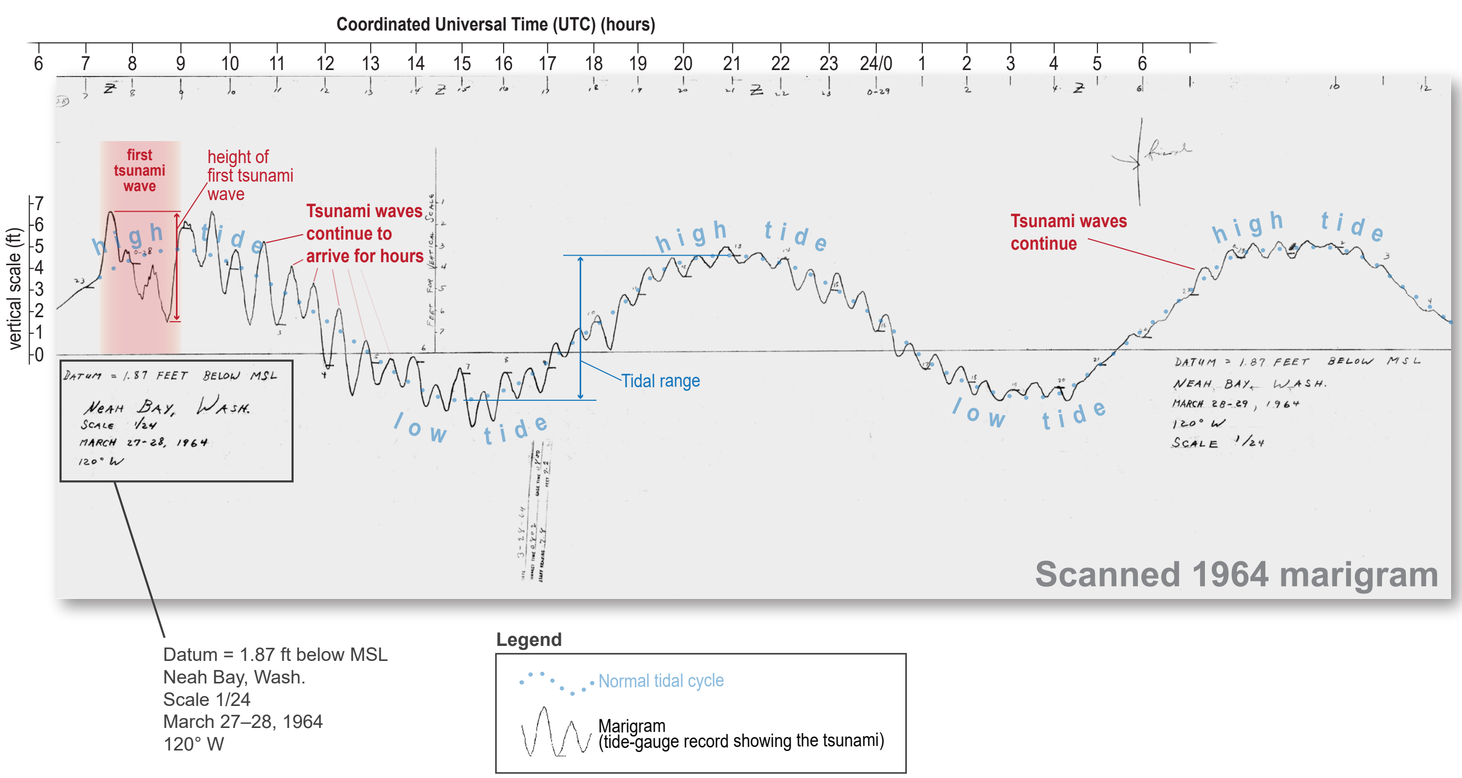

Figure 3. Neah Bay marigram (a printed recording of tide levels) capturing tsunami wave arrival at Neah Bay from the 1964 Alaska-Aleutian subduction zone event. The initial rising tsunami wave arrived on a rising tide just after 0700 am UTC (11 pm PST). Image from National Centers for Environmental Information (NCEI). We enhanced the archival image to improve its legibility.

Figure 4. Damage to a medium-sized home in the town of Pacific Beach, Washington, from tsunami inundation during the 1964 Great Alaska Earthquake. The home was lifted from its foundation and a portion of the house was torn away. The entire house moved northwest 40 ft (12.2 m) from its foundation and parts of the yard were eroded and covered with debris. Photo from Hogan and others (1964).

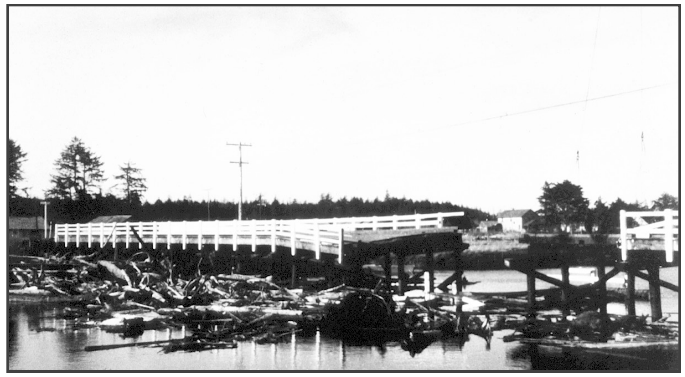

Figure 5. Destruction of the Highway 109 Copalis River Bridge, following tsunami inundation from the 1964 Great Alaska Earthquake. Two spans were lost, and timbers were bent. Two other 20-ft (6.1 m) spans are shown considerably deflected. Photo from Hogan and others (1964).

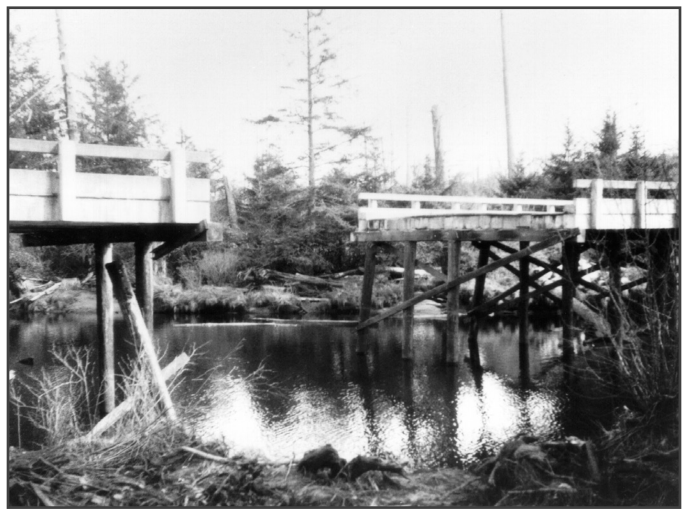

Figure 6. Destruction of Highway 109 Joe Creek Bridge, following tsunami inundation from the 1964 Great Alaska Earthquake. Pilings were lost, damaged, and bent. Two 20-ft (6.1 m) reinforced concrete spans were also lost. Photo from Hogan and others (1964).

on Washington State can be found in Walsh and others (2000). Damage to building foundations due to floating logs was reported in Pacific Beach (Fig. 4); timber-pile bulkheads and fill were extensively damaged in Moclips; several boats and a floating dock broke loose from moorings in La Push; and the loss of several skiffs and fish nets were reported at the mouth of the Quinault River in Taholah. There were also reports of damaged pilings near the Bone River Bridge on U.S. Highway 101 near Willapa Bay, and the adjacent Moore cannery building was lifted off its foundation and collided against the south approach of the bridge. As the tsunami continued to travel inland, buildings sustained water damage with standing-water depths ranging from 6 in. to several feet. Perhaps the most severe impacts took place along the Copalis River and State Highway 109. There, powerful waves entered the mouth of the Copalis River on the inflowing tide, destroying the Copalis River Bridge (Fig. 5) and the Joe Creek Bridge (Fig. 6). Also, along State Highway 109, 80 ft (24 m) of the road shoulder was eroded, and tsunami debris likely containing sediment and vegetation was deposited along the highway at Boone Creek. Erosion was also observed along the approach of the Wreck Creek Bridge and debris was deposited on the bridge deck and nearby highway (Hogan and others, 1964; Wilson and Torum, 1972; Walsh and others, 2000).

According to the Port Townsend Leader (1964), at Discovery Bay along the Strait of Juan de Fuca (Fig. 1), the tsunami caused two distinct episodes of flooding at the residence of Mrs. Audrey Bowman near the bank of Salmon Creek at the head of the bay. She reported that the first wave arrived at approximately 10:30 am UTC (2:30 am PST) and then receded after about 20 min. The second wave arrived at approximately 12 pm UTC (4:00 am PST), when Mrs. Bowman estimated the depth of the flooding to be approximately 6 ft (2 m) above the normal level of Salmon Creek. At the Crown Zellerbach paper mill in Port Townsend, a freighter ship rose 6–7 ft on the 'flood tide' though no damage was reported. At Quilcene Bay in the Hood Canal, a log raft was broken before being retrieved over the weekend (Port Townsend Leader, 1964). Within Discovery Bay, on the north bank of Salmon Creek, ~30 cm (~1 ft) below the surface, there is a 1–2-mm-thick (less than 0.1-in-thick) lamina of mud to very fine sand attributed to the 1964 event (Garrison-Laney and Miller, 2017). This thin layer is also present in core C-21 of Williams and others (2005). This is the only known location in Washington State where preserved tsunami deposits from the 1964 tsunami have been documented.

While this study does not consider the impacts of seiches, they were extensively reported during the 1964 Great Alaska Earthquake. Seiches are oscillations on the surface of a body of water caused by seismic waves originating from distant sources (McGarr and Vorhis, 1968). This oscillation can last for minutes to hours and can cause sloshing that may flood areas around the water body and damage infrastructure such as docks. Surface seismic waves (Love and Rayleigh waves) can travel much faster than a tsunami. Seismic seiching within Washington State was detected at tide and water-level stations following the 1964 earthquake (McGarr and Vorhis, 1968). More recently, on November 3, 2002, an M_W 7.9 earthquake in Denali, Alaska, generated a seiche in Lake Union in Seattle which damaged at least 20 houseboats, similar to damage sustained from seiching induced by the 1964 event (Barberopoulou and others, 2006). Washingtonians and visitors near shorelines of lakes, semi-enclosed bodies of water (such as harbors and marinas), rivers, and pools may experience sloshing waves immediately after another AASZ earthquake of similar size.

Recurrence Intervals of AASZ Earthquakes

The AASZ is an extensive subduction zone capable of generating significant large-magnitude earthquakes that impact local communities and those across the Pacific basin. For the purposes of this study, we are only considering recurrence of events on the AASZ between the Shumagin Islands and Cape Yakataga. The 1964 earthquake has been the only earthquake greater than magnitude 9 observed on the AASZ since the introduction of modern monitoring instruments. The coseismic deformation produced by the 1964 earthquake locally induced uplift or subsidence of coastal sediments (Plafker, 1969), depending on their distance from the megathrust fault. In order to estimate the recurrence of previous great earthquakes (> M_W 8.0) in south-central Alaska, paleoseismic investigations at coastal sites (for example, Carver and Plafker, 2008; Shennan and others, 2014; DePaolis and others, 2024; Barclay and others, 2024) have dated geologic evidence of sudden uplift or subsidence and found it occurs every ~600 yrs on average (Briggs and others, 2024).

METHODS AND MODELING

Earthquake Scenario Selection

The NOAA Center for Tsunami Research at the Pacific Marine Environmental Laboratory (PMEL) in Seattle conducted a series of tsunami wave simulations with different source functions formed from combinations of slip over various sub-faults, a method known as a disaggregated source analysis. This analysis determined which sources would produce the greatest tsunami energy directed towards Washington's waterways (Fig. 7; Chamberlin and others, 2009). In our study, we used the AASZ

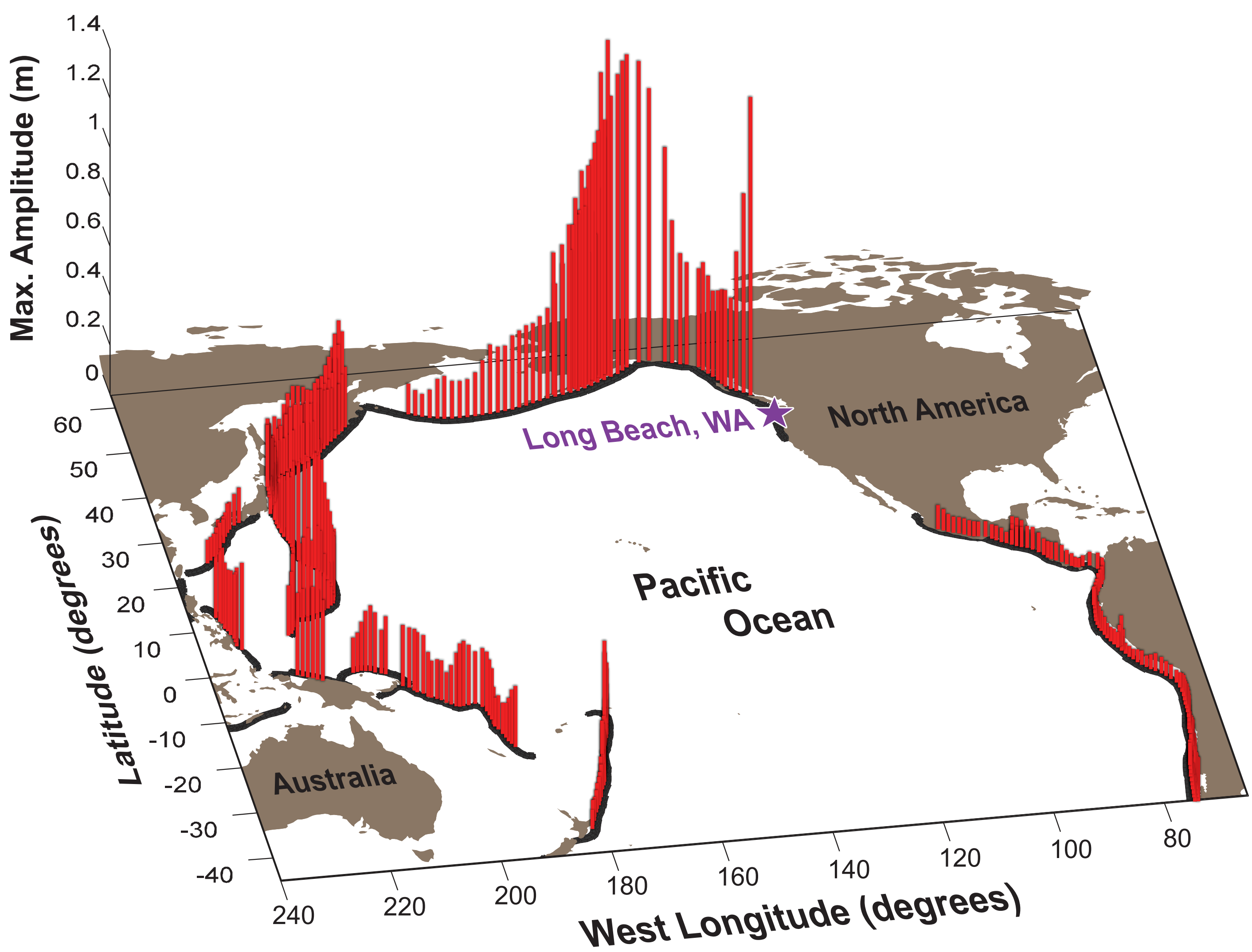

Figure 7. Maximum tsunami wave amplitudes offshore Long Beach, Washington (purple star), for 422 hypothetical M_W 9.2 earthquakes on subduction zones around the Pacific Ocean basin. Figure reproduced with permission from Chamberlin and others (2009).

earthquake scenario PMEL identified as posing the greatest threat to Washington (denoted as Scenario 1 by Chamberlin and others, 2009). This earthquake scenario exhibits uniform slip of 65.6 ft (20 m) over a set of 20 sub-faults represented as rectangular slip patches originating from the NOAA SIFT propagation database (Fig. 6; Gica and others, 2008; http://sift.pmel.noaa.gov/ComMIT/compressed/info_sz.dat). This slip produces a maximum uplift of ~33 ft (~9.7 m) and maximum subsidence of ~16 ft (~4.9 m), both of which occur instantaneously in our model. Horizontal motion and dynamic earthquake rupture were not used in the tsunami model. Since Scenario 1 focuses the greatest wave energy toward Washington as shown in Figure 9, we consider it the maximal M_W 9.2 distant-source event for Washington. Earthquakes larger than M_W 9.2 may be possible on the AASZ (Suleimani and others, 2022), but we did not consider them for this study because earthquake deformation sources for these larger events were not available at the time this project was initiated. Additionally, the selected source does not model splay fault ruptures, as these have been shown to not influence distant-source tsunami propagation (Suleimani and Freymueller, 2020).

Topography and Bathymetry

For simulating tsunami waves across the ocean basin, we used bathymetry with resolutions ranging from 1 arc-minute to 1/3 arc-second (NOAA National Geophysical Data Center, 2003; 2009; 2012; 2014; 2015; NOAA National Centers for Environmental Information, 2022a; 2022b). For tsunami modeling on land, we use high-resolution Digital Elevation Model (DEM) grids provided by NOAA's National Centers for Environmental Information (NOAA National Geophysical Data Center, 2011; 2014; 2015; Cooperative Institute for Research in Environmental Sciences (CIRES) at the University of Colorado, Boulder, 2025). Each grid cell on land within these DEM grids consists of either 1/3 or 1/9 arc-second spacing in both the longitude and latitude directions, but all have been down-sampled to 1/3 arc-second spacing (~23 ft (~7 m) east-west and ~33 ft (~10 m) north-south resolution) appropriate for regional tsunami inundation modeling.

We use 'bare-earth' DEMs, meaning that they do not include engineered structures, buildings, or trees. When tsunami waves interact with land, they also interact with all the vegetation and structures. These generally slow down the wave and reduce inundation extent. But both vegetation and the built environment can locally channelize flow and increase inundation depth and current speed. At present it is computationally impractical to

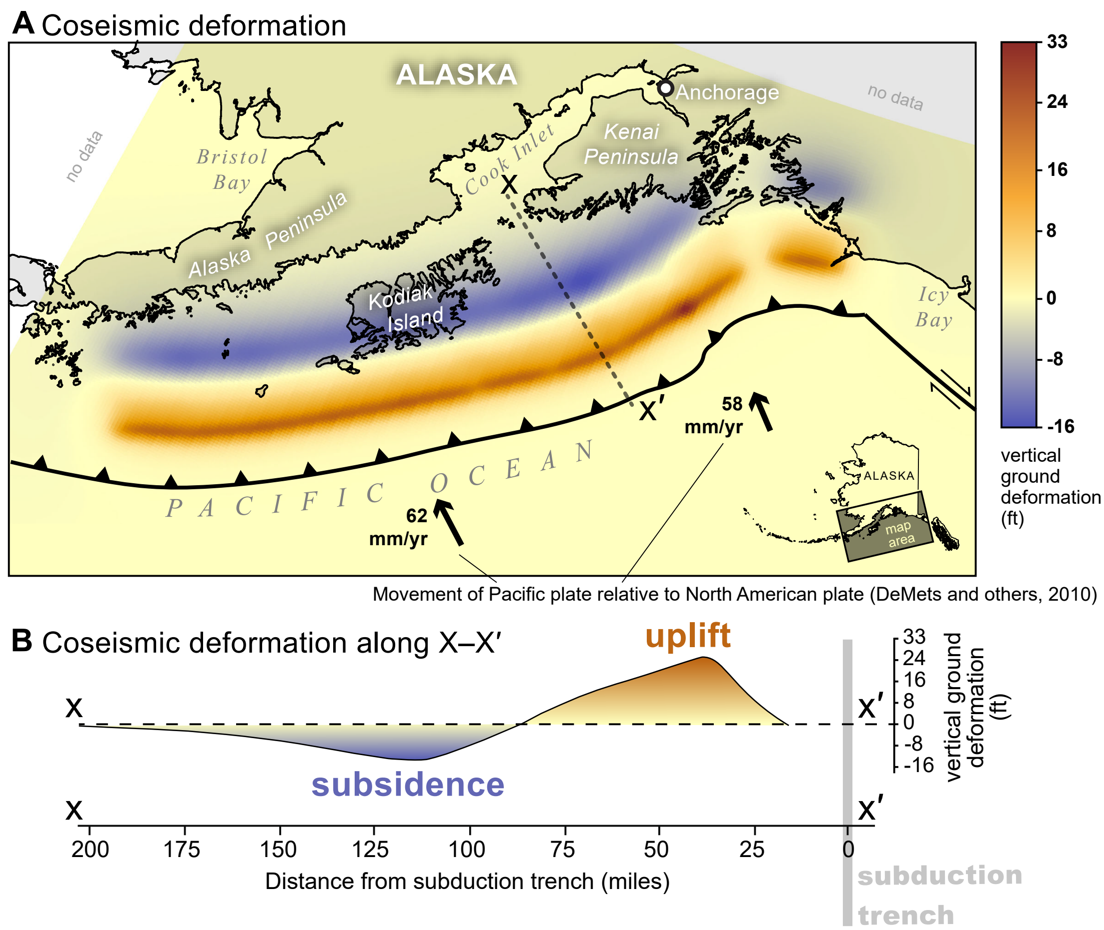

Figure 8. (A) Surface deformation for the AASZ earthquake scenario used in our modeling. The scenario was developed by the NOAA Center for Tsunami Research (Chamberlin and others, 2009). This earthquake scenario has a maximum uplift of ~33 ft (9.7 m) and maximum subsidence of ~16 ft (4.9 m). Plate motions were calculated based on the UNAVCO GAGE Plate Motion Calculator using the MORVEL 2010 model (DeMets and others, 2010). (B) Surface deformation along X–X′.

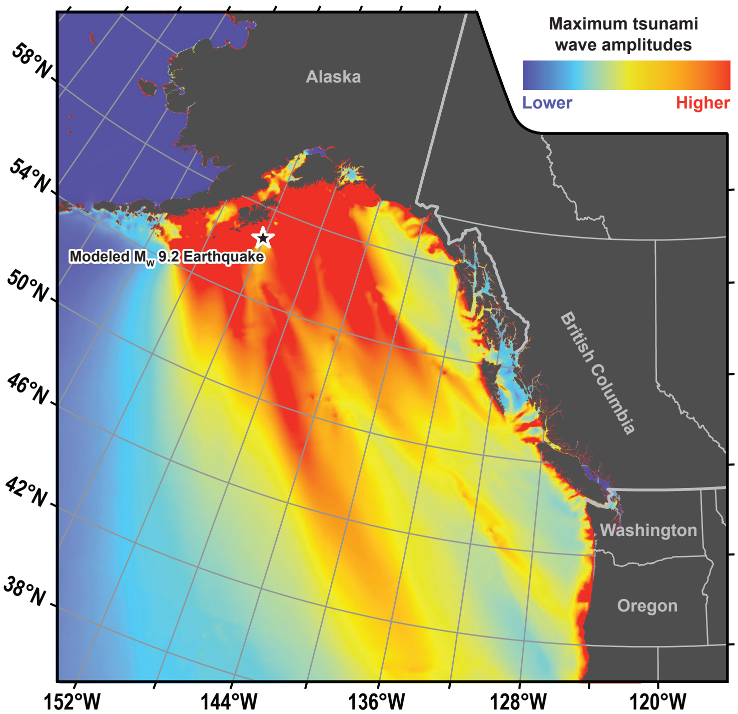

Figure 9. Modeled tsunami maximum wave amplitudes from earthquake Scenario 1 of Chamberlin and others (2009) utilized in this study. Wave amplitudes are commonly used as a proxy for propagation and directivity of wave energy.

complete the detailed modeling necessary to consider all buildings and vegetation. Additionally, buildings and vegetation will be modified or removed by the advance and retreat of tsunami waves and may be different in the future with land use changes along the coast. Instead, we model using the bare-earth DEM and assume a slight roughness to the land surface. Roughness is parameterized by the manning coefficient. We use a manning coefficient of 0.025 to 0.03 everywhere except in central Puget Sound, where we use 0.04 to represent a more densely built environment.

With this approach, modeled inundation likely has slightly greater extents and faster currents than a model that incorporates vegetation and built environment. Site-specific studies are recommended where the effects of vegetation or the built environment are important for planning and structural design.

Upriver bathymetry is limited by the availability of datasets such as single- and multi-beam sonar, soundings, and low-flow or low-tide lidar, which allow for visualization of the land surface under the water column. In most cases these datasets only exist within navigable channels and are thus limited to the largest rivers reaching the ocean (for example, the Columbia, Willapa, and Chehalis rivers). Beyond the navigable channel, or for smaller rivers and streams, the DEM is 'hydroflattened,' which is a technique in which the river is depicted as a relatively flat surface with elevations tied to each adjacent shoreline. Upstream water propagation is not simulated accurately on hydroflattened rivers due to the loss of the river channel, which is a significant pathway for water. While most upriver propagation would be constrained to the river's channel, there may be locations where near-channel wetlands and other low-lying areas may be flooded and are not shown as such in our inundation model.

Numerical Tsunami Modeling

The tsunami modeling included in this publication uses two numerical models: the Method of Splitting Tsunami (MOST) and GeoClaw. MOST was developed by PMEL and the University of Southern California (Titov and Synolakis, 1995; 1998; Titov and González, 1997). GeoClaw is an open-source code that is part of the Clawpack software that was initiated at the University of Washington (UW) and is still being developed by the UW tsunami modeling group, in collaboration with other contributors (Clawpack Development Team, 2025). Both packages solve the same set of nonlinear shallow-water equations that simulate tsunami generation, propagation, and inundation given specific earthquake and bathymetry inputs. Their main difference is in the numerical method employed.

The MOST package uses a grid of topographic and bathymetric elevations and calculates a water-surface elevation and velocity for each cell at specified time intervals. MOST applies a finite-difference numerical scheme to solve the nonlinear shallow water equations (Titov and others, 2016). This model also uses a set of three nested grids, referred to as A, B, and C grids, which become smaller in area and successively finer in resolution closer to the region of interest.

The GeoClaw package uses a finite-volume method that solves the nonlinear shallow-water wave equations (George 2006; 2008; George and LeVeque, 2006; Berger and others, 2011; LeVeque and others, 2011; Mandli and others, 2016). The model uses an Adaptive Mesh Refinement strategy to calculate water-surface elevations and velocities on a fine grid covering the region of interest and monitors the maximum values over the full simulation time.

MOST and GeoClaw have both been validated through benchmark tests and are approved by the National Tsunami Hazard Mitigation Program (NTHMP) for use in developing tsunami inundation models (Synolakis and others, 2007; González and others, 2011; Horrillo and others, 2015). To test how well the two software packages agree, a comparative study for Bainbridge Island, Washington showed generally excellent agreement between results from GeoClaw and MOST (Titov and others, 2018). To most efficiently use limited computing resources, and because the outputs from GeoClaw and MOST are similar, we used them interchangeably. Figure 10 shows which areas were modeled by either MOST or GeoClaw with some overlap between modeled areas. While this represents some duplication of effort, it was necessary to ensure that no data gaps were created between modeling teams and to adequately initialize tsunami flow to other parts of the study area. Where overlap between the models exists, we choose to retain the more conservative (higher) value of inundation depth or current speed.

The tsunami models use grids with both coarse and fine resolutions ranging from 1 degree to 1/3 arc-second. In some study areas, the transition from coarser to finer grids happens nearer to the shoreline than ideal and produces erroneously higher or lower inundation values than if the transition occurs farther offshore. In the complex waterways of the Salish Sea, this occurs in several areas where the transitional boundary does not cover the entirety of a bay or waterway. We solve this by having overlapping study areas, which allows for the dataset

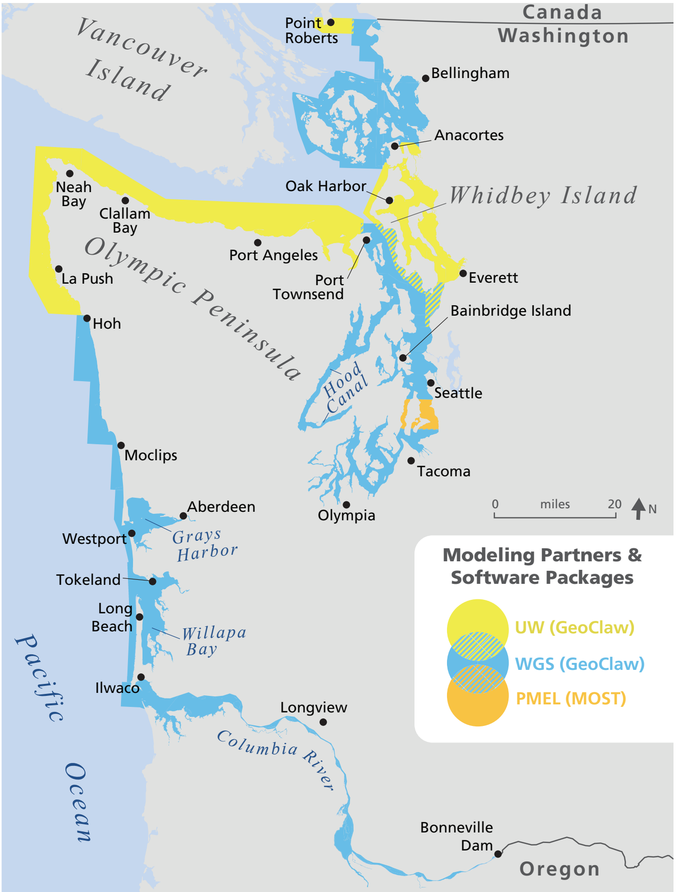

Figure 10. Modeling software and sources used in this publication. Colors on the map indicate areas modeled by either the Tsunami Modeling Group at the University of Washington (UW), the NOAA Center for Tsunami Research at the Pacific Marine Environmental Laboratory (PMEL), or the Washington Geological Survey (WGS). Regions of overlap used a compilation of all corresponding model results, prioritizing the maximum values. Both UW and WGS used the GeoClaw tsunami modeling software package while PMEL used the Method of Splitting Tsunami (MOST). Areas striped with two colors, for example on the west side of Whidbey Island, are areas that were modeled by two groups, in this case both UW and WGS.

with the more accurate coarse to fine transition to be used in compilation mapping.

Vertical Reference Datum

The vertical reference datum for all DEMs and tsunami simulation results is the mean high water (MHW) tidal datum. This reference point stays static throughout the simulation as if the tsunami arrives (and stays at) high tide throughout the course of the simulation. For example, the difference in height between MHW and mean lower low water (MLLW) is 9.14 ft (2.79 m) at Westport, Washington (NOAA, 2025). Were the tsunami inundation model run at MLLW the overall tsunami inundation would be considerably lower given the lower tide stage. Thus, the inundation results included in this study are higher when compared to tsunami models that use a lower static tide stage. Select examples of this comparison are available via the Tsunami Maritime Resilience Strategies by Washington Emergency Management Division (https://mil.wa.gov/tsunami).

Sea Level Change, Tidal Currents, and Riverine Flow

The contributions of projected sea-level rise to tsunami inundation were also not explored in this study. Global sea level rise may force a change in future vertical reference datums. Future studies, such as site-specific tsunami modeling for structural design, should exercise caution when comparing tsunami model results where the vertical reference datum has changed.

The tsunami model used in this study does not include river discharge or tidal currents. The interaction between a tsunami and currents can be additive if in the same direction, thereby generating greater flooding. Where tidal currents or river discharge flow against the incoming tsunami, it may steepen the tsunami wave front, causing a breaking wave commonly referred to as a bore (Zhang and others, 2011).

Earthquake Source Limitations

Tsunami models have assumptions and technical limitations that generate uncertainties on the accuracy of the tsunami model outputs compared to a real tsunami. The largest single source of uncertainty in the tsunami model originates from the earthquake source. Rupture patterns of earthquakes on a given subduction zone often vary significantly (Petersen and others, 2023), and it is possible that a large AASZ earthquake may generate a tsunami where the brunt of impact misses the Washington Coastline, as happened in 1964. Our selected source aims to reduce the impact of this uncertainty by rupturing a part of the subduction zone with the greatest directivity toward Washington (Fig. 9).

Additional uncertainty is introduced through the use of the Okada model, which simplifies the subduction geometry, takes the input of slip on a rectangular patch, and produces deformation of the earth surface (Okada, 1985). This deformation is expressed as a static vertical component of seafloor displacement for tsunami generation. This scenario ruptures instantaneously in our modeling along the AASZ margin and does not include other potential components that could alter tsunami generation, such as material heterogeneity in the subduction zone, inelastic behavior, horizontal displacement, splay or trench-breaching faulting within the subduction zone, or dynamic coseismic deformation. The earthquake source utilized in this study crosses up to five major AASZ segments that have highly variable coupling of 50–100 percent (Briggs and others, 2024). A real earthquake generated in the same section of the subduction zone will have a more complex slip distribution and rupture geometry than this modeled scenario.

RESULTS

We modeled the entire 3,026-mi-long (4,870 km) Washington coastline for an M_W 9.2 Alaska-Aleutian Subduction Zone event using the MOST and GeoClaw tsunami modeling software packages. The results of the modeling indicate that an M_W 9.2 earthquake along the AASZ could generate a tsunami capable of causing significant damage to Washington State. The compiled model results include wave arrival times, inundation depths and extents, and directional current speeds (velocity). We provide the data as a Data Supplement (https://fortress.wa.gov/dnr/geology-data/tsunami_models/WGS_Washington_AK9p2_model_data.zip) which contains:

1. Model results in TIFF format including inundation depths and current speeds for all of Washington's coastal waterways.

2. A post-processed inundation extent as an ESRI polygon feature class within a geodatabase.

3. Technical modeling reports from each modeling partner for the modeled areas shown in Figure 7. Summary figures of maximum offshore wave amplitudes, current speeds, and first tsunami wave arrival times are included within these modeling reports.

Results Summary

The modeled tsunami arrival times, nearshore amplitudes, and current speeds are depicted in Figures 11, 12, and 13 respectively. Additional detailed data in GIS format are available in the Data Supplement. The tsunami reaches La Push first, 3 h and 30 min after the earthquake. The tsunami arrives in Shelton last, 7 h and 40 min after the earthquake. The greatest inundation occurs along the Grayland, Westport, and Ocean Shores peninsulas, Kalaloch and other beaches in the Olympic National Park, and at the tribal communities of Taholah, Hoh, La Push, and Neah Bay. Areas east of the mouth of the Strait of Juan de Fuca generally have less than 8 ft (2.4 m) of inundation depth at the shoreline. Areas of Puget Sound and the northern Strait of Georgia generally experience less than 5 ft (1.5 m) of inundation depth except in select locations, such as the heads of bays like Bellingham Bay, Eastsound, and Lynch Cove where tsunami waves coalesce and push inundation depths up to 14 ft (4.3 m). The highest current speeds are found along the outer coast, exceeding 9 kn (4.6 m/s) at the Long Beach, Grayland, Westport, and Ocean Shores peninsulas, and at the tribal communities of Taholah, Hoh, La Push, and Neah Bay. Elsewhere the currents are generally less than 9 kn except where flow is constricted through narrow passageways such as in the San Juan Islands, Guemes Channel and the entrance to Port Gamble.

Wave Arrival

The estimated wave arrival times listed in Table 1 and in the Data Supplement correspond to the first change from the mean high water (MHW) tidal datum. This change from normal is a rising (cresting) wave for all locations included in this study due to the geometry of the AASZ and dynamics of earthquake rupture (see Fig. 7). It takes approximately 3 h and 30 min after the earthquake and tsunami generation for the first tsunami wave to reach La Push, Washington, along the outer coast. The tsunami reaches all points along the outer coast in less than 3 h and 45 min. The leading wave continues to propagate inland, into Grays Harbor and Willapa Bay, and up the Columbia River, as well as into the Strait of Juan de Fuca. The leading wave continues traveling south into Puget Sound and north into the Strait of Georgia to the Canadian border. Figure 9 and Table 1 summarize the arrival of the first tsunami wave for locations on the inner and outer coasts. Tsunami waves may continue for

Table 1. Summary of approximate first tsunami wave arrival and maximum offshore wave amplitude for select locations included in this study. The first modeled wave is a rising, inundating wave for all locations. Locations are listed in order of first wave arrival. Maximum offshore amplitude may not coincide with the first wave arrival because the first tsunami wave may not be the largest.

Location	Approximate First Wave Arrival (hours:minutes after earthquake)	Approximate Maximum Offshore Amplitude (ft)
La Push	3:30	13
Hoh	3:35	19
Long Beach	3:35	19
Waatch	3:40	15
Neah Bay	3:40	7
Queets	3:40	14
Taholah	3:40	15
Westport	3:40	24
Moclips	3:45	16
Oregon/Washington Border	3:45	7
Port Angeles	4:00	7
Tokeland	4:00	3
South Bend	4:05	3
Whidbey Island	4:10	5
Port Townsend	4:10	8
Aberdeen	4:25	5
Friday Harbor	4:50	3
Eastsound	4:55	10
Anacortes	4:55	4
Bangor	4:55	3
Skamokawa	5:00	2
Cherry Point	5:05	3
Blaine	5:30	4
Bellingham	5:35	9
Hoodsport	5:35	4
Stanwood	5:40	4
Everett	5:40	2
Seattle	5:40	2
Bremerton	5:45	3
La Conner	5:50	2
Lynch Cove	5:55	14
Oak Harbor	6:00	4
Port of Tacoma	6:00	5
Gig Harbor	6:05	4
Nisqually	6:20	2
Olympia	7:00	4
Shelton	7:40	2

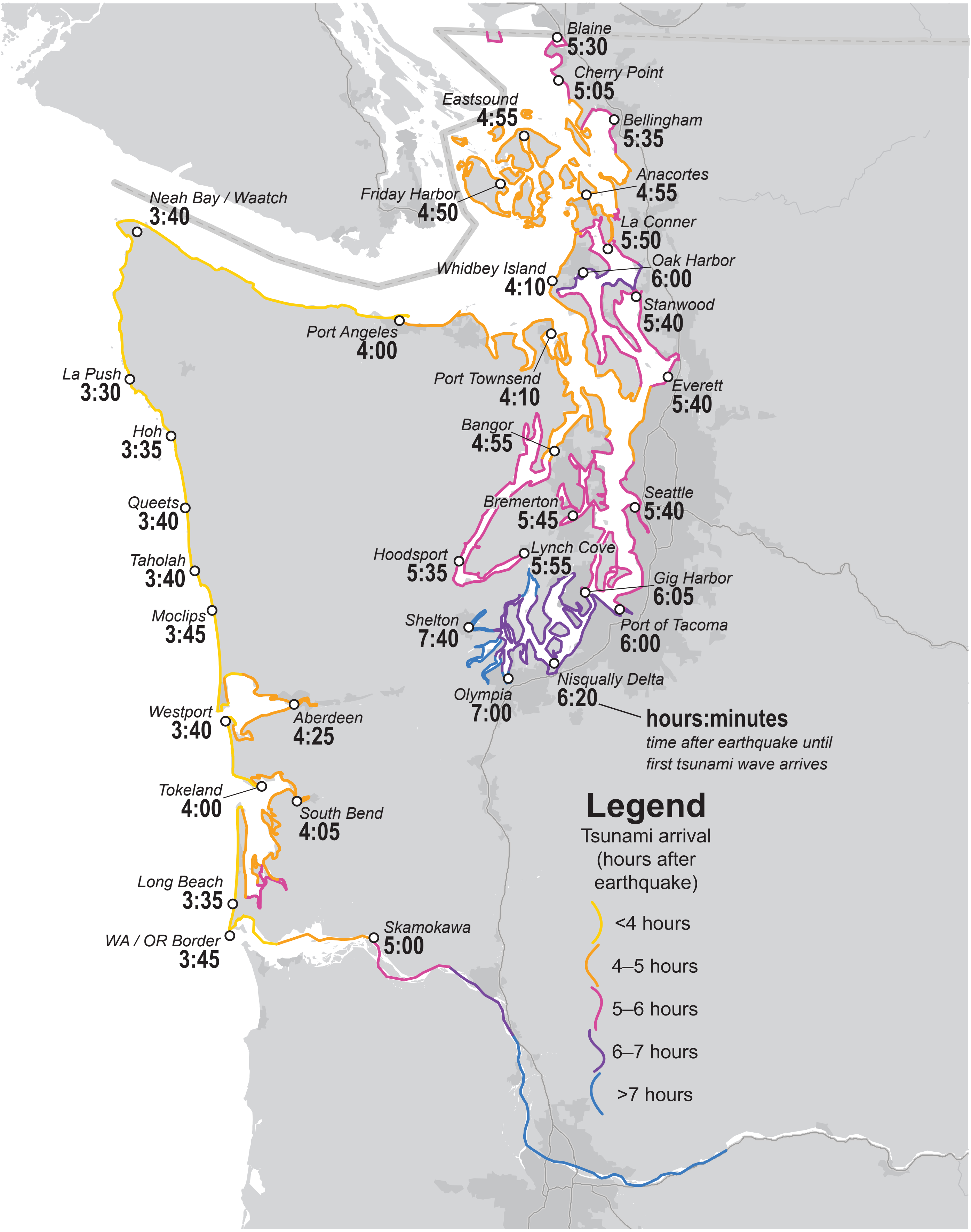

Figure 11. Tsunami travel times from source (also referred to as 'arrival times') in hours:minutes following an AASZ earthquake. Estimated tsunami travel times are also shown in Table 1.

24 h or more and the first wave may not be the largest. In the 1964 Great Alaska Earthquake, the most destructive wave in Willapa Bay (near South Bend; Fig. 11) occurred about 12 h after the first wave reached Washington (Walsh and others, 2000), approximately 15.5 h after the earthquake.

Maximum Offshore Wave Amplitude and Onshore Inundation Depth

Modeled offshore wave amplitudes, measured as the height of the rising wave above the MHW datum, are dependent on offshore depth. In the open ocean, tsunami waves go largely undetected except by specifically designed instrumentation known as Deep-ocean Assessment and Reporting of Tsunamis (DART) sensors. However, as the tsunami approaches the shoreline, water depths become shallower, and the tsunami amplitude becomes larger. This is because a tsunami waveform differs from that of traditional wind waves in that wind waves impact only surface water while tsunamis involve the whole water column. During tsunami propagation, as seafloor depth decreases, wave amplitudes increase. This effect is known as shoaling.

Along the coast of Washington at selected synthetic tide gauges (Fig. 12, and in the Data Supplement) offshore wave amplitudes are provided to give an estimate of how high the waves are as they approach land. On the Pacific Ocean coast, wave amplitudes near the shoreline are 14–24 ft (4.3–7.3 m), with the greatest amplitude recorded in the Westport area. Within Grays Harbor, Willapa Bay, and the Columbia River estuary, wave amplitude decreases to 2–5 ft (0.6–1.5 m). As the tsunami waves propagate along the shorelines of the Strait of Juan de Fuca, they maintain a 7–8 ft (2.1–2.4 m) amplitude until reaching Puget Sound. Within the inner waterways of Puget Sound and into the Strait of Georgia the amplitudes decrease to 2–5 ft (0.6–1.5 m) except at the end of elongated bays and coves such as near Lynch Cove, Eastsound, and Bellingham, where wave shoaling amplifies waves to heights of 9–14 ft (2.7–4.3 m), often corresponding with the first rising (cresting) wave.

In addition to offshore wave amplitudes, the model results in the Data Supplement provide onshore inundation depths (denoted as flow depth), which is the depth of flooding water above previously dry land, and the inundation extent of the tsunami waves. Note that offshore wave amplitude does not correlate directly to onshore inundation depths because factors such as local topography have major influences on onshore flooding.

Our modeling shows that a tsunami generated by an M_W 9.2 AASZ earthquake would inundate many low-lying regions in Washington. The model inundation results show the most severe onshore flooding in southwest Washington along the Ocean Shores, Grayland, and Tokeland peninsulas. There, tsunami inundation depths reach as much as 10 ft (3 m) up to a quarter mile inland. This depth of inundation also occurs at Lynch Cove at the end of Hood Canal. Onshore tsunami inundation depths are generally less than 4 ft for most of Puget Sound. This is due to the relatively low wave amplitudes that propagate into the region and limited shoaling. The modeled tsunami does flow a significant distance up many rivers and along their floodplains despite these low wave amplitudes due to many rivers in Puget Sound, Grays Harbor, and Willapa Bay, as well as along the Columbia River, having low elevation profiles. The tsunami model does not include river outflow, which would flow against the tsunami and reduce its upriver propagation.

Maximum Current Speeds

Tsunami current velocity is a measure of the speed and directionality of the water movement during the tsunami. Both the GeoClaw and MOST tsunami models track directionality and speed of the tsunami as it propagates through Washington's waterways and over land. Over the duration of a tsunami, the maximum speed value is recorded for a given location. Current velocity is a critical dataset for the maritime industry, which often has supporting infrastructure that is exposed to tsunamis. The modeled speeds can be compared to the port damage categorization of Lynett and others (2014), which roughly predicts damage to vessels and infrastructure based on current speeds (Table 2).

Areas with modeled current speeds of greater than 3 kn (shown in Fig. 13) should be considered the minimum extent of area impacted by potentially hazardous currents. Adjustments in the model setup such as changing tidal datums, model resolution, or adding dynamic tides can cause whirlpools (vortices) and high-speed flows to take slightly different paths as demonstrated in the Washington State Tsunami Maritime Resilience Strategies (Washington State Military Department Emergency Management Division, 2021; 2022; 2024a; 2024b; 2024c; 2025). As a result, the spatial extents of vortices and high-speed flow paths anticipated from a real event likely encompass a wider area than shown in Figure 13. Model results for current speeds as well as momentum flux (depth × speed^2) are available in the Data Supplement.

Certain topographic or engineered features, like entrances into harbors or marinas, typically have faster currents than the surrounding areas. Additionally, small islands, land spits with narrow passageways, or bathymetric features such as shoals and rocks may also impact current speeds and form vortices. Tidal currents have shown to increase maximum tsunami speeds up to 25 percent (Ayca and Lynett, 2016) indicating that locations that experience fast tidal currents are also likely to experience the higher current speeds during a tsunami.

In a few places within Puget Sound, modeled current speeds locally exceed 9 kn (4.6 m/s), placing them within the maximum anticipated damage category of Lynett and others (2014). These locations include Agate Passage, Deception Pass, Rich Passage, Port Gamble, and the southern end of Hood Canal east of Union (Fig. 13). Areas exceeding 9 kn (4.6 m/s) can also be found within northern Puget Sound. These locations include: the narrow channels of the San Juan Islands, Guemes Channel, Hale Passage, and Scow Bay. These potentially damaging current speeds are

Table 2. Damage categorization of Lynett and others (2014) with modified values for vessels and infrastructure older than 40–50 yrs (Pat Lynett, personal communication).

Damage Anticipated	Speed (kn) against newer vessels / infrastructure	Speed (kn) against older vessels / infrastructure
None	0–3	0-2
Minor to Moderate	3-6	2-5
Major	6-9	5-7
Extreme	>9	>7

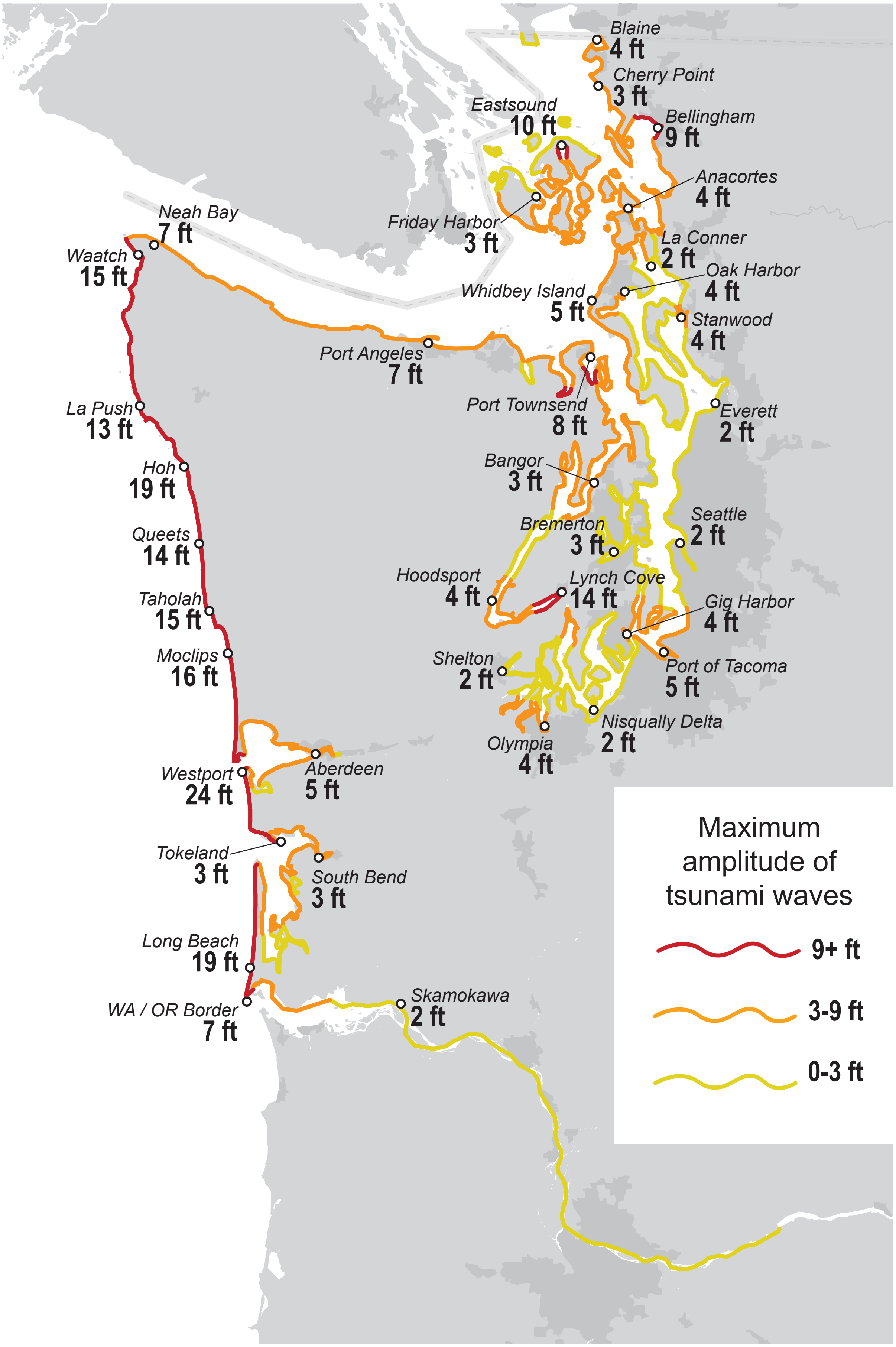

Figure 12. Maximum tsunami wave amplitudes at selected localities along coastal Washington. Note that the largest tsunami wave may not be the first to arrive. These values are also shown in Table 1.

Figure 13. Map of coastal Washington showing areas where tsunami current speeds exceed 3 kn, indicating areas where damage may be expected and marine navigation would be difficult. High-speed areas may exist farther offshore along the outer coast of Washington than is depicted on this figure as we only show modeled currents up to one mile from the shoreline.

also present along much of the shoreline of the outer coast and the mouth of the Columbia River. Our modeled current-speed values reflect only tsunami forces and do not include any tidal current speeds. If tidal currents are flowing in the direction of the tsunami, then their speeds should be accounted for in our modeled speeds for a more accurate reflection of what total current speed in an area could be. Overland current speeds alone don't determine damage, as inundation depth is also a key factor. Both tsunami current speeds and onshore inundation depths are needed to calculate momentum-flux forces, which help determine impacts on structures (American Society of Civil Engineers, 2022). These calculations can be derived from the Data Supplement.

IMPLICATIONS FOR PUBLIC SAFETY

Shaking from a distant-source earthquake may not be felt in Washington. Thus, timely and effective alerts and messaging are needed so that people can take protective action before the tsunami arrives. Fortunately, tsunami waves generated from the modeled AASZ earthquake scenario would not reach Washington until several hours after the earthquake. Tsunami alert messages originate from the National Tsunami Warning Center (NTWC), located in Palmer, Alaska. The NTWC disseminates these messages to the National Weather Service (NWS), the United State Coast Guard (USCG), the Federal Emergency Management Agency (FEMA), the Washington State Emergency Operation Center (SEOC), tribes, and local jurisdictions. Tsunami alerts may also be broadcasted through NOAA weather radios, over cellular networks by means of a Wireless Emergency Alert (WEA) message, and through All Hazard Alert Broadcast Sirens (AHAB). Still, the possibility of missing an official alert exists, and it is crucial to recognize any natural warning signs of an incoming distant tsunami from Alaska. These may include a loud roar coming from the ocean, water levels increasing faster than any tide, water surging toward the shore, or extreme shifts in currents. Note that a tsunami originating from the AASZ differs to one originating from the Cascadia Subduction Zone (CSZ). During a CSZ tsunami, modeling shows that in most places the water would initially recede from the shoreline, providing a warning of the arriving tsunami (Dolcimascolo and others, 2021; 2022). However, because of the orientation of the AASZ relative to Washington, the first sign of an AASZ tsunami for Washington would be a rising wave.

Surviving a tsunami is possible with proactive planning. This includes knowing where the inundation zones are and if you're in one (or not) when you receive a tsunami alert. If you are in the inundation zone, know how to reach high ground quickly and have a general awareness of any reinforced buildings or structures that are specifically designed to be resistant to earthquakes and tsunamis. As a last resort, seek out trees or other obstacles to stand behind to avoid the direct impact of objects entrained in the water. Atwater and others (2005) provide general information for surviving a tsunami based on historical events. Additionally, Washington Emergency Management Division provides Washington-specific information and guidance on tsunami emergency preparedness.

ACKNOWLEDGMENTS

We would like to thank the National Tsunami Hazard Mitigation Program (NTHMP) for supporting a portion of the modeling included in this project, in cooperation with cities, counties, tribes, and the Washington Emergency Management Division. Tsunami modeling for this project also includes NOAA PMEL contribution 5364. We acknowledge the work of the Washington Geological Survey (WGS) publications staff: Nikolas Midttun for editing and typesetting the pamphlet and contributing to figure development; Daniel Coe for his feedback in figure development and for producing the statewide tsunami simulation video accompanying this project; Ashley Cabibbo and Keara McLean for making the data packages publicly available and updating the WGS Geologic Information Portal (geologyportal.dnr.wa.gov); and Susan Schnur for her keen eye in editing and meaningful feedback throughout this project. We would like to acknowledge the computing time provided by the University of Colorado Community Surface Dynamics Modeling System (CU-CSDMS) High-Performance Computing Cluster, and by the Applied Mathematics Department at the University of Washington. We are also extremely thankful for peer reviews by Barrett Salisbury, Elena Troshina, and SeanPaul La Selle which greatly improved this publication.

AUTHOR CONTRIBUTIONS

The tsunami models and accompanying technical reports were completed by A. Dolcimascolo (Washington Geological Survey), R. LeVeque and L. Adams (University of Washington), and V. Titov, C. Moore, and D. Arcas (NOAA PMEL). D. Eungard compiled the digital data deliverable. A. Dolcimascolo and D. Eungard led the writing of the pamphlet, and A. Steely contributed significantly during the editing process.

REFERENCES

American Association of Highway and Transportation Officials (AASHTO), 2022, Guide specifications for bridges subject to tsunami effects: American Association of Highway and Transportation Officials, 56 p.

Atwater, B. F.; Cisternas, V. M.; Bourgeois, Joanne; Dudley, W. C.; Hendley, J. W., II; Stauffer, P. H., 2005, Surviving a tsunami—Lessons from Chile, Hawaii, and Japan: U.S. Geological Survey Circular 1187, v. 1.1, 18 p. [https://pubs.usgs.gov/circ/c1187/]

American Society of Civil Engineers, 2022, Tsunami loads and effects. Chapter 6 In American Society of Civil Engineers, Minimum design loads and associated criteria for buildings and other structures: Structural Engineering Institute of the American Society of Civil Engineers, ASCE/SEI 7-22, p. 25–54. [https://doi.org/10.1061/9780784415788]

Ayca, Aykut; Lynett, P. J., 2016, Effect of tides and source location on nearshore tsunami-induced currents: Journal of Geophysical Research: Oceans, v. 121, no. 12, p. 8,807–8,820. [https://doi.org/10.1002/2016JC012435]

Barberopoulou, Aggeliki; Qamar, Anthony; Pratt, T. L.; Steele, W. P., 2006, Long-period effects of the Denali earthquake on water bodies in the Puget Lowland: Observations and modeling: Bulletin of the Seismological Society of America, v. 96, no. 2, p. 519–535. [https://doi.org/10.1785/0120050090]

Barclay, D. J.; Haeussler, P. J.; Witter, R. C., 2024, Dating the penultimate great earthquake in south-central Alaska using tree-ring crossdating and radiocarbon wiggle-matching: Quaternary Science Advances, v. 13, 100142. [https://doi.org/10.1016/j.qsa.2023.100142]

Berger, M. J.; George, D. L.; LeVeque, R. J.; Mandli, K. T., 2011, The GeoClaw software for depth-averaged flows with adaptive refinement: Advances in Water Resources, v. 34, no. 9, p. 1,195–1,206. [https://doi.org/10.1016/j.advwatres.2011.02.016]

Briggs, Rich; Witter, R. C.; Freymueller, J. T.; Powers, P. M.; Haeussler, P. J.; Ross, S. L.; Dura, Tina; Engelhart, S. E.; Koehler, R. D.; Thio, H. K., 2024, An Alaska–Aleutian subduction zone interface earthquake recurrence model from geology and geodesy. In Ruppert, N. A.; Jadamec, M. A.; Freymueller, J. T., editors, Tectonics and Seismic Structure of Alaska and Northwestern Canada: American Geophysical Union, p. 299–323. [https://doi.org/10.1002/9781394195947.ch10]

Brocher, T. M.; Filson, J. R.; Fuis, G. S.; Haeussler, P. J.; Holzer, T. L.; Plafker, George; Blair, J. L., 2014, The 1964 Great Alaska Earthquake and tsunamis—A modern perspective and enduring legacies: U.S. Geological Survey Fact Sheet 2014-3018, 6 p. [https://dx.doi.org/10.3133/fs20143018]

Carver, Gary; Plafker, George, 2008, Paleoseismicity and neotectonics of the Aleutian subduction zone—An overview. In Freymueller, J. T.; Haeussler, P. J.; Wesson, R. L.; Ekström, Göran, editors, Active tectonics and seismic potential of Alaska: American Geophysical Union Geophysical Monograph Series 179, p. 43–63. [https://doi.org/10.1029/179GM03]

Chamberlin, C. D.; Titov, V. V.; Arcas, Diego, 2009, Modeling tsunami inundation impact on the Washington coast from distant seismic sources: Pacific Marine Environmental Laboratory, 27 p.

Clawpack Development Team, 2025, Clawpack software versions 5.5.0–5.10.0. [https://doi.org/10.17605/osf.io/kmw6h]

Cooperative Institute for Research in Environmental Sciences (CIRES) at the University of Colorado, Boulder, 2025, Continuously updated digital elevation model (CUDEM)—1/9 arc-second resolution bathymetric-topographic tiles, coastal Washington 2020–2025: NOAA National Centers for Environmental Information. [accessed Jan. 14, 2025 at https://www.ncei.noaa.gov/access/metadata/landing-page/bin/iso?id=gov.noaa.ngdc.mgg.dem:199919]

DeMets, Charles; Gordon, R. G.; Argus, D. F., 2010, Geologically current plate motions: Geophysical Journal International, v. 181, p. 1–80. [https://doi.org/10.1111/j.1365-246X.2009.04491.x]

DePaolis, J. M.; Dura, Tina; Witter, R. C.; Haeussler, P. J.; Bender, Adrian; Curran, J. H.; Corbett, D. R., 2024, Repeated coseismic uplift of coastal lagoons above the Patton Bay splay fault system, Montague Island, Alaska, USA: Journal of Geophysical Research: Solid Earth, v. 129, no. 5, e2023JB028552. [https://doi.org/10.1029/2023JB028552]

Dolcimascolo, Alexander; Eungard, D. W.; Allen, Corina; LeVeque, R. J.; Adams, L. M.; Arcas, Diego; Titov, V. V.; Gonzalez, F. I.; Moore, Christopher; Garrison-Laney, C. E.; Walsh, T. J., 2021, Tsunami hazard maps of the Puget Sound and adjacent waters-Model results from an extended L1 Mw 9.0 Cascadia subduction zone megathrust earthquake scenario: Washington Geological Survey Map Series 2021-01, 16 sheets, scale 1:48,000, 49 p. text. [https://fortress.wa.gov/dnr/geologydata/tsunami_hazard_maps/ger_ms2021-01_tsunami_hazard_puget_sound.zip]

Dolcimascolo, Alexander; Eungard, D. W.; Allen, Corina; LeVeque, R. J.; Adams, L. M.; Arcas, Diego; Titov, V. V.; Gonzalez, F. I.; Moore, Christopher; Garrison-Laney, C. E.; Walsh, T. J., 2022, Tsunami hazard maps of the Olympic Peninsula-Model results from an extended L1 Mw 9.0 Cascadia subduction zone megathrust earthquake scenario: Washington Geological Survey Map Series 2022-01, 14 sheets. [https://fortress.wa.gov/dnr/geologydata/tsunami_hazard_maps/ger_ms2022-01_tsunami_hazard_olympic_peninsula.zip]

Garrison-Laney, Carrie; and Miller, Ian, 2017, Tsunamis in the Salish Sea: Recurrence, sources, hazards. *In* Haugerud, R. A.; Kelsey, H. M., eds., From the Puget Lowland to east of the Cascade Range: Geologic excursions in the Pacific Northwest: Geological Society of America Field Guide 49, p. 67–78. [https://doi.org/10.1130/2017.0049(04)]

George, D. L., 2006, Finite volume methods and adaptive refinement for tsunami propagation and inundation: University of Washington Doctor of Philosophy thesis, 167 p. []

George, D. L., 2008, Augmented Riemann solvers for the shallow water equations over variable topography with steady states and inundation: Journal of Computational Physics, v. 227, no. 6, p. 3,089–3,113. [https://doi.org/10.1016/j.jcp.2007.10.027]

George, D. L.; LeVeque, R. J., 2006, Finite volume methods and adaptive refinement for global tsunami propagation and local inundation: Science of Tsunami Hazards, v. 24, no. 5, p. 319–328. [http://tsunamisociety.org/245george.pdf]

Gica, Edison; Spillane, M. C.; Titov, V. V.; Chamberlin, C. D.; Newman, J. C., 2008, Development of the forecast propagation database for NOAA's Short-term Inundation Forecast for Tsunamis (SIFT): NOAA Technical Memorandum OAR PMEL-139, 89 p. [https://www.pmel.noaa.gov/pubs/PDF/gica2937/gica2937.pdf]

González, F. I.; LeVeque, R. J.; Chamberlain, Paul; Hirai, Bryant; Varkovitsky, Jonathan; George, D. L., 2011, Validation of the GeoClaw model—NTHMP MMS tsunami inundation model validation workshop: University of Washington, 84 p. [https://depts.washington.edu/clawpack/links/nthmp-benchmarks/geoclaw-results.pdf]

Hogan, D. W.; Whipple, W. W.; Lundy, C., 1964, Tsunami of 27 and 28 March, 1964, State of Washington coastline: U.S. Army Corps of Engineers [Seattle, Washington], unpublished file report, 29 p.

Horrillo, Juan; Grilli, S. T.; Nicolsky, Dmitry; Roeber, Volker; Zhang, Joseph, 2015, Performance benchmarking tsunami models for NTHMP's inundation mapping activities: Pure and Applied Geophysics, v. 172, no. 3–4, p. 869–884. [https://doi.org/10.1007/s00024-014-0891-y]

Lander, J. F.; Lockridge, P. A.; Kozuch, M. J., 1993, Tsunamis affecting the west coast of the United States, 1806–1992: National Geophysical Data Center Key to Geophysical Records Documentation No. 29, 242 p. [https://repository.library.noaa.gov/view/noaa/13442/noaa_13442_DS1.pdf]

LeVeque, R. J.; George, D. L.; Berger, M. J, 2011, Tsunami modelling with adaptively refined finite volume methods: Acta Numerica, v. 20, p. 211–289. [https://doi.org/10.1017/S0962492911000043]

Lynett, P. J.; Borrero, Jose; Son, Sangyoung; Wilson, Rick; Miller, Kevin, 2014, Assessment of the tsunami-induced current hazard: Geophysical Research Letters, v. 41, no. 6, p. 2048–2055. [https://doi.org/10.1002/2013GL058680]

Mandli, K. T.; Ahmadia, A. J.; Berger, Marsha; Calhoun, Donna; George, D. L.; Hadjimichael, Yiannis; Ketcheson, D. I.; Lemoine, G. I.; LeVeque, R. J., 2016, Clawpack: Building an open source ecosystem for solving hyperbolic PDEs: PeerJ Computer Science, v. 2, no. e68, 27 p. [https://doi.org/10.7717/peerj-cs.68]

McGarr, Arthur; Vorhis, R. C., 1968, Seismic seiches from the March 1964 Alaska earthquake: U.S. Geological Survey Professional Paper 544–E, 1 sheet, scale 1:5,000,000, with 43 p. text. [https://pubs.usgs.gov/pp/0544e/]

National Oceanic and Atmospheric Administration (NOAA), 2025, Datums for 9441102, Westport WA [webpage]: NOAA. [accessed Jan. 14, 2025 at https://tidesandcurrents.noaa.gov/datums.html?id=9441102]

National Geophysical Data Center/World Data Service, 2025, NCEI/WDS Global Historical Tsunami Database [webpage]: NOAA National Centers for Environmental Information. [accessed Sept. 11, 2025 at https://doi.org/10.7289/V5PN93H7].

NOAA National Centers for Environmental Information, 2022a, ETOPO 2022 15 arc-second global relief model—Tiled 15 arc-second ice surface elevation netCDF [GIS data]: NOAA National Centers for Environmental Information. [https://doi.org/10.25921/fd45-gt74]

NOAA National Centers for Environmental Information. 2022b, ETOPO 2022 30 arc-second global relief model—30 arc-second ice surface elevation netCDF [GIS data]: NOAA National Centers for Environmental Information. [https://doi.org/10.25921/fd45-gt74]

NOAA National Geophysical Data Center, 2003, U.S. coastal relief model vol. 8—Northwest Pacific [GIS data]: NOAA National Centers for Environmental Information. [https://doi.org/10.7289/V5H12ZXJ]

NOAA National Geophysical Data Center, 2009, ETOPO1 1 arc-minute global relief model [GIS data]: NOAA National Centers for Environmental Information. [https://doi.org/10.7289/V5C8276M]

NOAA National Geophysical Data Center, 2011, Port Townsend, Washington 1/3 arc-second MHW coastal digital elevation model [GIS data]: NOAA National Centers for Environmental Information. [accessed Aug. 31, 2011 at https://www.ncei.noaa.gov/metadata/geoportal/rest/metadata/item/gov.noaa.ngdc.mgg.dem:1786/html].

NOAA National Geophysical Data Center, 2012, Astoria, Washington 1/3 arc-second MHW coastal digital elevation model [GIS data]: NOAA National Centers for Environmental Information, [accessed Aug. 28, 2012 at https://www.ngdc.noaa.gov/thredds/catalog/regional/catalog.html?dataset=regionalDatasetScan/astoria_13_mhw_2012.nc]

NOAA National Geophysical Data Center, 2014, Puget Sound, Washington 1/3 arc-second MHW coastal digital elevation model [GIS data]: NOAA National Centers for Environmental Information. [accessed Oct. 22, 2014 at https://www.ncei.noaa.gov/metadata/geoportal/rest/metadata/item/gov.noaa.ngdc.mgg.dem:5165/html].

NOAA National Geophysical Data Center, 2015, Strait of Juan de Fuca, Washington 1/3 arc-second NAVD88 coastal digital elevation model [GIS data]: NOAA National Centers for Environmental Information. [accessed Oct. 22, 2015 at https://www.ncei.noaa.gov/metadata/geoportal/rest/metadata/item/gov.noaa.ngdc.mgg.dem:11514/html].

Okada, Yoshimitsu, 1985, Surface deformation due to shear and tensile faults in a half-space: Bulletin of the Seismological Society of America, v. 75, no. 4, p. 1135–1154. [https://doi.org/10.1785/BSSA0750041135]

Petersen, M. D.; Shumway, A. M.; Powers, P. M., 2023, The 2023 US 50-State National Seismic Hazard Model: Overview and implications: Earthquake Spectra, v. 40, no. 1, 88 p. [https://doi.org/10.1177/87552930231215428]

Plafker, George, 1969, Tectonics of the March 27, 1964 Alaska earthquake: U.S. Geological Survey Professional Paper 543-I, 74 pp. [https://doi.org/10.3133/pp543I]

Plafker, George; Kachadoorian, Reuben, 1966, Geologic effects of the March 1964 earthquake and associated seismic sea waves on Kodiak and nearby islands, Alaska: U.S. Geological Survey Professional Paper 543-D, 46 p. [https://doi.org/10.3133/pp543D]

Port Townsend Leader, 1964 (2 April), Tidal wave alerts received by various agencies here: Port Townsend Leader [newspaper], v. 76, no. 14, p. 1.

Shennan, Ian; Bruhn, Ronald; Barlow, Natasha; Good, Kelly; Hocking, Emma, 2014, Late Holocene great earthquakes in the eastern part of the Aleutian megathrust: Quaternary Science Reviews, Vol. 84, p. 86–97. [https://doi.org/10.1016/j.quascirev.2013.11.010]

Suleimani, Elena; Freymueller, J. T., 2020, Near-field modeling of the 1964 Alaska tsunami: The role of splay faults and horizontal displacements: Journal of Geophysical Research: Solid Earth, v. 125, no. 7, e2020JB019620. [https://doi.org/10.1029/2020JB019620]

Suleimani, E. N.; Salisbury, J. B.; Nicolsky, D. J., 2022, Updated tsunami inundation maps for Karluk and Larsen Bay, Kodiak Island, Alaska: Alaska Division of Geological & Geophysical Surveys Report of Investigation 2022-2, 42 p., 2 sheets. [https://doi.org/10.14509/30892]

Suleimani, Elena, 2011,Numerical Studies Of Tectonic And Landslide-Generated Tsunamis Caused By The 1964 Great Alaska Earthquake: University of Alaska Doctor of Philosophy thesis, 181 p. [https://ualaska.researchcommons.org/uaf_grad_geosci/199]

Synolakis, C. E.; Bernard, E. N.; Titov, V. V.; Kânoğlu, Utku; González, F. I., 2007, Standards, criteria, and procedures for NOAA evaluation of tsunami numerical models: National Oceanic and Atmospheric Administration Technical Memorandum OAR PMEL-135, 55 p. [https://repository.library.noaa.gov/view/noaa/11073/noaa_11073_DS1.pdf]

Titov, V. V.; Arcas, Diego; Moore, C. W.; LeVeque, R. J.; Adams, L. M.; González, F. I., 2018, Tsunami hazard assessment of Bainbridge Island, Washington—Project Report: Washington State Emergency Management Division, 43 p. [http://depts.washington.edu/ptha/WA_EMD_Bainbridge/BainbridgeIslandTHA.pdf].

Titov, V. V.; Kânoğlu, Utku; Synolakis, C. E., 2016, Development of MOST for real-time tsunami forecasting: Journal of Waterway, Port, Coastal, and Ocean Engineering, v. 142, no. 6, 48 p. [https://doi.org/10.1061/(ASCE)WW.1943-5460.0000357]

Titov, V. V.; Gonzalez, F. I., 1997, Implementation and testing of the Method of Splitting Tsunami (MOST) model: NOAA Technical Memorandum ERL PMEL-112 (PB98-122773), 11 p. [https://www.pmel.noaa.gov/pubs/PDF/tito1927/tito1927.pdf]

Titov, V. V.; Synolakis, C. E., 1995, Modeling of breaking and nonbreaking long-wave evolution and runup using VTCS-2: Journal of Waterway, Port, Coastal, and Ocean Engineering, v. 121, no. 6, p. 308–316. [https://doi.org/10.1061/(ASCE)0733-950X(1995)121:6(308)]

Titov, V. V.; Synolakis, C. E., 1998, Numerical modeling of tidal wave runup: Journal of Waterway, Port, Coastal, and Ocean Engineering, v. 124, no. 4, p. 157–171. [https://doi.org/10.1061/(ASCE)0733-950X(1998)124:4(157)]

Walsh, T. J.; Caruthers, C. G.; Heinitz, A. C.; Myers, E. P., III; Baptista, A. M.; Erdakos, G. B.; Kamphaus, R. A., 2000, Tsunami hazard map of the southern Washington coast—Modeled tsunami inundation from a Cascadia subduction zone earthquake: Washington Division of Geology and Earth Resources Geologic Map GM-49, 1 sheet, scale 1:100,000, with 12 p. text. [http://www.dnr.wa.gov/publications/ger_gm49_tsunami_hazard_southern_coast.zip]

Washington State Military Department Emergency Management Division, 2021, Tsunami maritime response and mitigation strategy—Port of Bellingham, Bellingham, Washington, 75 p. [https://mil.wa.gov/asset/60ad926bdefd6]

Washington State Military Department Emergency Management Division, 2022, Tsunami maritime response and mitigation strategy—Westport Marina, Port of Grays Harbor, Westport, Washington, 76 p. [https://mil.wa.gov/asset/655e368ef222f/Westport%20Marina%20Report%20New%20Cover.pdf]

Washington State Military Department Emergency Management Division, 2024a, Tsunami maritime response and mitigation strategy—City of Bainbridge Island's Eagle Harbor, Bainbridge Island, Washington: Washington Emergency Management Division, 107 p. [https://mil.wa.gov/asset/67646c4307dc1/City%20of%20Bainbridge%20Island%20Eagle%20Harbor%20TMRMS.pdf]

Washington State Military Department Emergency Management Division, 2024b, Tsunami maritime response and mitigation strategy—The Port of Anacortes, Anacortes, Washington: Washington Emergency Management Division, 98 p. [https://mil.wa.gov/asset/66608fac3bb11/Port%20of%20Anacortes%20Tsunami%20Maritime%20Strategy_Revised.pdf]

Washington State Military Department Emergency Management Division, 2024c, Tsunami maritime response and mitigation strategy—Makah Tribe's Port of Neah Bay, Neah Bay, Washington: Washington Emergency Management Division, 99 p. [https://mil.wa.gov/asset/6709b20ff34bb/Makah%20Tribe%20Port%20of%20Neah%20Bay%20Tsunami%20Maritime%20Strategy.pdf]

Washington State Military Department Emergency Management Division, 2025, Tsunami maritime response and mitigation strategy: Port Angeles and John Wayne Marina, Port Angeles and Sequim, Washington: Washington Emergency Management Division, 119 p. [https://mil.wa.gov/asset/6930ae6a8bcb8/251202_Port-Angeles-and-John-Wayne-Marina-Tsunami-Maritime-Strategy-FINAL.pdf]

Wesson, R. L.; Boyd, O. S.; Mueller, C. S.; Bufe, C. G.; Frankel, A. D.; Petersen, M. D., 2007, Revision of time-independent probabilistic seismic hazard maps for Alaska: U.S. Geological Survey Open-File Report 2007-1043, 33 p. [https://doi.org/10.3133/ofr20071043]

Wilson, B. W.; Torum, Alf, 1972, Runup heights of the major tsunami on North American coasts. *In* National Research Council Committee on the Alaska Earthquake, The Great Alaska Earthquake of 1964—Oceanography and coastal engineering: National Academy of Sciences, p. 158-180.

Williams, H. F. L.; Hutchinson, Ian; Nelson, A. R., 2005, Multiple sources for late-Holocene tsunamis at Discovery Bay, Washington State, USA: The Holocene, v. 15, no. 1, p. 60–73. [https://doi.org/10.1191/0956683605hl784rp]

Zhang, Y. J.; Witter, R. C.; Priest, G. R., 2011, Tsunami–tide interaction in 1964 Prince William Sound tsunami: Ocean Modelling, v. 40, no. 3–4, p. 246–259. [https://doi.org/10.1016/j.ocemod.2011.09.005]